

A new insight into morphological, thermal, and mechanical properties of melt-processed polylactide/poly(ϵ -caprolactone) blends

Orebotse Joseph Botlhoko^{a,b}, Suprakas Sinha Ray^{a,b*} and James Ramontja^{a*}

^aCentre for Nanomaterials Science Research, Department of Applied Chemistry, University of Johannesburg, Doornfontein 2028, Johannesburg, South Africa.

^bDST-CSIR National Centre for Nanostructured Materials, Council for Scientific and Industrial Research, Pretoria 0001, South Africa.

*Corresponding authors. E-mail addresses: jamesr@uj.ac.za (JR); rsuprakas@csir.co.za (SSR) ssinharay@uj.ac.za (SSR)

Highlights

- PLA/PCL blends with different compositions are processed using melt-blending.
- **The relationship between the** obtained morphology and properties is reported.
- Unique thermal stability of dispersed phase improves the degradation of blends.
- 60PLA/40PCL blend shows significantly improved thermal stability and mechanical properties.
- The results inform technologically advanced PLA-based materials for commercial applications.

ABSTRACT: Biodegradable polylactide (PLA)/poly(ϵ -caprolactone) (PCL) blend is a well-studied immiscible polymer blend system; however, there is no fundamental understanding of how the dispersed phase morphology controls the thermal stability, and the thermal and mechanical properties of the blend systems. Addressing this research question, a series of PLA/PCL blends were processed using melt-blending technique. The results show that the unique thermal stability of the dispersed PCL domains prolonged the complete degradation process of PLA. Furthermore,

altering the activation energies (E_a) of PLA/PCL blends revealed that thermal stability depends not only on the governing mechanism change during degradation process but also on the behavior of phase-separated morphology characteristics. The presence of evenly dispersed PCL particles within PLA matrix enhanced the crystallization rate coefficient of PLA and tailored the spherulite morphologies by acting as a nucleating agent, thus promoting the crystallization ability of PLA chains. Consequently, remarkable increase in elongation at break was achieved for 60PLA/40PCL blend, with well-balance tensile modulus and tensile strength characteristics. Despite the significant storage modulus increase of the blends at low temperatures, significant storage modulus decrease is noted with increasing temperature, due to packing density, chain mobility phenomenon, and unfrozen PCL molecules. The enhanced processability of PLA by ductile PCL, with improved and balanced properties, enables the technological advancement of bio-based PLA for a wide range of applications.

KEYWORDS: polylactide/poly(ϵ -caprolactone) immiscible blends, thermal degradation kinetics, crystallization behavior, material and mechanical properties

1. Introduction

In the family of bio-based biodegradable polymers, polylactide (PLA) is the most promising sustainable substitute for conventional polymers, due to its well-balanced mechanical and materials properties [1,2]. Consequently, there is growing interest in PLA for various eco-friendly packaging and medical applications. However, its inherent brittleness, low impact strength and melt strength, slow crystallization kinetics, and lower thermal stability during high temperature processing **as well as the thermal degradation kinetics characteristics** all limit the use of pure PLA for large-scale commercial applications [4–7].

In this context, blending PLA with more ductile biodegradable polymers **with good thermal degradation kinetics characteristics and the ability to create a platform to effectively nucleate PLA** **have** attracted significant industrial and academic research interest in order to widen its

applications [8]. In this regard, blends of PLA with highly flexible and biodegradable polymers, such as poly(ϵ -caprolactone) (PCL), poly[(butylene succinate)-co-adipate] (PBSA), poly(butylene succinate) (PBS), poly(glycolide) (PGA), etc., have been extensively investigated with the dual objectives of addressing the brittleness of PLA and improving the inherent material properties [2, 9–16].

Among these, PCL has attracted greater interest due to its remarkable elongation at break ($\geq 400\%$), low glass transition temperature, and exclusive thermal stability associated with its high thermal degradation activation energy (E_a) and crystallization characteristics when combined with a PLA matrix [8,11,17,18]. On the other hand, the lower melting temperature, tensile modulus, and tensile strength limit the extensive use of pure PCL. However, many studies revealed that PLA/PCL blends show immiscibility characteristics over a range of compositions [7,19,20]. In most cases, one component fundamentally benefits the polymer blend system by its ability to nucleate the other component, through interface-assisted nucleation mechanism or migration of one component to another during melt-processing. In addition, the homogeneity of droplet spherulite morphologies also plays a key role in nucleation. On the other hand, higher loading of either PCL or PLA component can cause droplets to coalesce, thus producing a PLA/PCL blend with co-continuous morphology. Moreover, this relationship is associated with the viscoelastic properties of matrices and droplet percolation [6]. This implies that crystallization kinetics, polymer composition, and surface morphology play vital roles in controlling the properties of the desired material as well as the interfacial tension, processing condition, and rheological properties of the components [10]. However, prior to setting processing conditions, practically applying polymeric materials, and in order to hypothesize the thermal recyclization of a particular polymeric blend system, scientists/engineers must systematically understand the thermal degradation behavior of the polymeric materials [11]. This highlights the objective of the current study. Several studies have reported on the morphology and thermal properties of PLA/PCL blend systems as well as their compatibilization effect by the use of polymeric compatibilizers and

nanofillers [14, 21–24]. For example, Todo *et al.* [14] reported that the addition of PCL particles to PLA/PCL blends activated PLA crystallinity, although the system still demonstrated immiscible phenomenon. In addition, it should be mentioned that rapid crystallization rates during processing enable faster molding cycles, thereby saving energy and reducing production times. Sivalingam and Madras [11] investigated the thermal degradation of PCL, PLA, and PGA, which showed peak decomposition temperatures at approximately 402, 360, and 295 °C, respectively. PCL, PGA, and PLA were reported to degrade by both random chain scission and specific chain end scission. Moreover, PCL exhibited more E_a than PGA and PLA, at 18.5, 16.5, and 10.2 kcal mol⁻¹, respectively. However, that study did not relate the observed thermal degradation results with morphology and bond interaction or any other properties. Moreover, Mitchel and Hirt [25] reported E_a value of PLA at about 26.3 kcal mol⁻¹, while Mofokeng and luyt [26] reported E_a value of PCL at about 131 KJ mol⁻¹. With this rationale in mind, in the present study, prior to investigating the role of PCL in the crystallization behavior and thermal degradation kinetics of PLA matrix, PLA/PCL compositions were first processed using industrially favorable melt-blending method instead of plasticization or co-polymerization, and then screened based on the mechanical and material properties. The optimized blend composition was selected based on the balanced thermal stability, mechanical properties, and outstanding elongation at break, while the blend system constitutes PLA as the matrix and PCL as the minor phase. Furthermore, extensive studies were conducted to gain a molecular-level understanding of the relationship between the thermal degradation kinetics and morphology of the optimum PLA/PCL blend. In addition, the roles of cooling rate on PLA/PCL crystallinity phenomenon, packing density, and polymer chain mobility in controlling the mechanical and material properties were studied. On the basis of the observed properties, the unique blend composition was selected for further development of high-performance, environmentally benign PLA-based blends for packaging and related applications.

2. Experimental

2.1. Materials

Commercial-grade PLA (PLA U'Z S-17) with a D-content of approximately 1 wt% was obtained from Toyota (Japan). The supplier specifies the following PLA characteristics: molecular weight (M_w) 120–135 kg mol⁻¹, density (ρ) 1.24 g cm⁻³, melt flow index (MFI) 15.84 g/10 min (190 °C/2.16 kg, according to the ISO 1133B standard method), glass transition temperature (T_g) 62 °C, and melting temperature (T_m) 175 °C. PCL was purchased from Sigma-Aldrich (South Africa), with M_w 80 kg mol⁻¹, ρ 1.145 g cm⁻³, MFI 5.57 g/10 min (190 °C/2.16 kg, according to the ISO 1133B standard method), and T_m 60 °C. Prior to use, PLA was dried at 80 °C, whereas PCL was dried at 40 °C under vacuum for 12 h.

2.2. Processing of PLA/PCL blends

PLA/PCL blends with various weight ratios (100/0, 90/10, 80/20, 70/30, 60/40, 50/50, 40/60, 30/70, 20/80, 10/90, and 0/100 wt%) were processed *via* melt-mixing in a HAAKE PolyLab OS Rheomix (Thermo Electron Co., USA) operated at a set temperature of 195 °C for 8 min with a screw speed of 60 rpm. The resulting blends were compression-molded into various specimens with a total residence time of 2 min at 195 °C using a Caver compression molder (Carver, USA, model 973214A). The applied pressure was 1.2 MPa. Finally, the samples were cooled to approximately 20 °C by passing tap water. The purely PLA and PCL samples were also processed in the same way as used for the blends. The dog-bone-shaped compression-molded samples (3 mm in thickness, 3.40 mm in width, and 25 mm in gauge length) were used for the tensile tests. On the other hand, compression-molded rectangular samples with dimensions of approximately 12.40, 9.90, and 1.70 mm (length, width, thickness) were used for the dynamic properties measurements.

2.3. Characterization

X-ray diffraction (XRD) experiments on the compression-molded samples of purely PLA or PCL, and their blends were conducted using an X'Pert PRO diffractometer (PANalytical, Netherlands)

producing Cu K α radiation ($\lambda = 1.54$ nm). Samples were scanned at a scan step of approximately 0.026°. The generator was operated at a voltage of 45 kV and a tube current of 40 mA.

The morphologies of the blend samples were analyzed using field-emission scanning electron microscopy (SEM) (JSM-7500, JEOL, Japan). Prior to imaging, the blend samples were freeze-fractured in liquid nitrogen, then the fractured surface was sputter-coated with carbon, and the sides were painted with a silver paste to reduce charging, and finally imaged at an acceleration voltage of 3 kV. To obtain more detailed insights into the morphology, the number-average radius (R_n) of PLA and PCL droplets for various samples was determined by imageJ software (ImageJ 1.46r), using equation 1.

$$R_n = \frac{\sum n_i R_i}{n_i} \quad (1)$$

Here, n_i is the number of dispersed droplets with a radius R_i counted. The Weibull model was used to fit the data obtained from equation 1.

The morphologies of the samples were further analyzed using a high-resolution transmission electron microscope (JEM2100, JEOL, Japan) operated at an acceleration voltage of 200 kV. Prior to analyses, the samples were prepared using a Leica (Austria) EM FC6, through ultramicrotomy at 27 °C, cutting speed of 3 mm s⁻¹, and feed rate of 90 nm, after which the specimens were embedded into copper 300 mesh regular grid with a diamond knife.

Thermogravimetric analysis (TGA) of the samples was performed using a TG analyzer (model Q500, TA Instruments, USA). Samples weighing approximately 10 mg were heated in platinum pans from about 30 to 900 °C at a scan rate of 10 °C min⁻¹ under nitrogen environment (flow rate = 20 ml min⁻¹). For each sample, the experiment was repeated at least three times, and the most representative result is reported. To obtain a more detailed understanding of the thermal degradation kinetics, TGA analyses were conducted at different heating rates of 5, 10, 15, and 20 °C min⁻¹ under nitrogen environment with a flow rate of 20 ml min⁻¹ from 30 to 650 °C. The E_a values of various samples were determined by the Kissinger method, using equation 2:

$$\ln\left(\frac{\beta}{T_m^2}\right) = \left(-\frac{E_a}{RT_m}\right) + \ln\left(\frac{AR}{E_{dm}}\right) \quad (2)$$

Here, β is the heating rate in $^{\circ}\text{C min}^{-1}$, E_a is the activation energy in KJ mol^{-1} , R is the universal gas constant ($8.314 \text{ J.Mol}^{-1}.\text{K}^{-1}$), T_m is the maximum degradation temperature in K , and A is the pre-exponential factor [27–29]. The mass conversion (α) is determined by equation 3

$$\alpha = \frac{W_o - W_t}{W_o - W_f} \quad (3)$$

where W_o is weight at initial degradation, W_t is weight at time t , and W_f is the final weight of the sample or reaction.

Differential scanning calorimetry (DSC) measurements of single polymer and blended samples (weighing approximately 5.6 mg using aluminum pans) were conducted using a DSC-Q2000 (TA Instruments, USA) within the temperature range -65 to 200 $^{\circ}\text{C}$ under a nitrogen atmosphere with a flow rate of $25 \text{ ml}\cdot\text{min}^{-1}$. The samples were tested at the same heating and cooling rate of 10 $^{\circ}\text{C}\cdot\text{min}^{-1}$ in three consecutive scans: heating, cooling, and heating. The first heating scan erased the previous thermal history of the samples, while the second heating scan was used to determine the cold crystallization temperature (T_{cc}), enthalpy of cold crystallization (ΔH_{cc}), T_m , and heat of fusion (ΔH_m). The cooling scan was used to determine crystallization temperature (T_c) and enthalpy of crystallization (ΔH_c). Equation 4 was used to calculate the degree of crystallinity (X_c). For each sample, the experiment was repeated at least three times and the most representative result is reported. For nonisothermal crystallization kinetic studies, each sample was cooled at various cooling rates of 5, 10, 15, and 20 $^{\circ}\text{C min}^{-1}$ from the melt to -65 $^{\circ}\text{C}$. As soon as cooling was finished each sample was heated to 200 $^{\circ}\text{C}$ at heating rates of 5, 10, 15, and 20 $^{\circ}\text{C min}^{-1}$.

$$\% \text{ Crystallinity } (X_c) = \frac{\Delta H_m}{\Delta H^{\circ}_m \times W_f} \times 100 \quad (4)$$

Where, ΔH_m is the specific melting enthalpy of each polymer phase in a sample, W_f is the weight fraction of each polymer within the sample, and ΔH°_m is the specific melting enthalpy of the 100% crystalline PLA and PCL, which are 93 [30] and 135 [31] J g^{-1} , respectively.

The morphology of the dispersed phase at the molten state, and spherulitic growth behavior of the selected samples were studied using a polarized optical microscope (POM). Compression-molded thin film of each sample was placed between two covering glasses, which were gently pressing together and subjected to a Linkam hot stage (Linkam Scientific Instruments, Ltd., UK) of the microscope. Isothermal crystallization was recorded by heating the sample to 200 °C and holding for 5 min, then cooling to 120 °C and holding for 20 min. Again, the spherulitic behavior of neat PCL was studied at 30 °C for 20 min.

Tensile tests were conducted using an Instron 5966 tester (Instron Engineering Corp., USA) with a load cell of 10 kN. The tests were performed to determine the mechanical properties of the samples under tension mode at a single strain rate of 5 mm min⁻¹ at 30 °C. The reported results are an average of at least six independent tensile test measurements.

The dynamic mechanical properties were studied using a PerkinElmer DMA 8000 analyzer (USA) under dual-cantilever bending mode. Analyses were conducted within the temperature range -90 to 90 °C at a heating rate of 2 °C min⁻¹. Each experiment was conducted at a constant frequency of 1 Hz with strain amplitude of 0.02%.

Melt-state dynamic rheological measurements were conducted using a Physica MCR501 (Anton Paar, Austria) rheometer equipped with parallel plates of 25 mm diameter, **results are reported in the supporting information**. Disc-shaped (thickness approximately 1.68 mm) compression-molded samples were used, and measurements were conducted at 190 °C under nitrogen environment, with strain amplitude of 1% and a zero gap of 1.15 mm. Steady shear measurements at increasing strain amplitude were conducted at a fixed frequency of 1 rad s⁻¹.

3. Results and discussion

3.1. Structural and morphological characteristics of PLA/PCL blends

Detailed chemical and structural characteristics of the neat polymers and their blends can be found in Fig. S1, Supporting Information. The XRD patterns of various samples are presented in Fig. 1.

The XRD pattern of neat PLA shows a diffraction peak at $2\theta \approx 16.35^\circ$, corresponding to 110 or 200 plane [31], whereas that of neat PCL shows two sharp diffraction peaks at $2\theta \approx 21.42^\circ$ and $\approx 23.73^\circ$ corresponding to 110 and 200 planes, with the shoulder peak at $2\theta \approx 21.90^\circ$ corresponding to 111 plane [32,33]. For the PLA/PCL blends, the XRD peak related to neat PLA ($2\theta \approx 16.35^\circ$) dissipated with increasing PCL content, suggesting that the crystallization of PLA is hindered by the higher amount of PCL. Whereas, the appearance at lower PCL content suggests that the crystallization of PLA is activated by the presence of low PCL content. Similar phenomenon was also reported by Mofokeng *et al.* [34] in poly(propylene)/low density polyethylene blend system as well as Todo *et al.* [14] in PLA/PCL blend system. Importantly, 40 wt% PCL is the maximum content required in order to possibly activate crystallization of PLA, this behavior it attributed to the interfacial area per unit volume exposed by the PCL. On the other hand, PCL-rich blends show prominent diffraction peaks without notable shift ($2\theta \approx 21.42, 21.90,$ and 23.73°), which reveals that the presence of a dispersed minor PLA phase has no apparent influence on the crystal structure and lamellar thickness of PCL due to immiscibility factors.

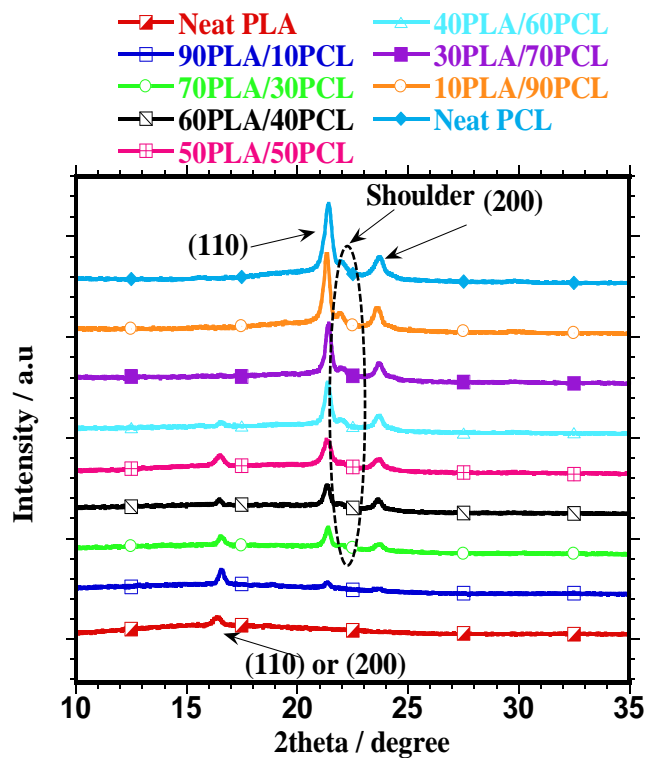


Fig. 1. XRD patterns of neat PLA, neat PCL, and various PLA/PCL blends.

The freeze-fracture surface morphologies studies of PLA/PCL blends presented in Fig. 2 reveal phase-separated morphology, indicating poor compatibility between PLA and PCL phases, thus immiscible characteristics [20]. The surface morphologies of the PLA and PCL phases in various blends were characterized using Image J software [Fig. 3(a)]. PLA droplets are smaller than those of PCL for respective opposite compositions (e.g., 80PLA/20PCL vs. 20PLA/80PCL compositions). In other words, PLA-rich blends show high number-average droplet size compared to PCL-rich blends (the droplet sizes for 10, 20, 30, and 40 wt% PCL are larger than those for 10, 20, 30, and 40 wt% PLA), as clearly indicated in Fig. 3(a). However, our observations differ from Ojijo *et al.* [9], who observed that PLA droplets had larger diameter than those of the respective opposite compositions in PLA/PBSA blend systems. They reported that the observed morphologies were due to the different volume fractions, differences in melt viscosities, and subsequent phase separation during annealing. In this study, the morphologies result from differences in viscosity ratio, $\eta_{\text{PCL}} > \eta_{\text{PLA}}$, discussed latter. It is well known that it is difficult to deform the droplets of the dispersed phase during mixing if the dispersed phase has higher viscosity than the matrix; as a result, larger PCL droplet size occurs. Furthermore, the lower T_m of PCL ($\text{PCL}_{T_m} < \text{PLA}_{T_m}$; $55.5\text{ }^\circ\text{C} < 176.9\text{ }^\circ\text{C}$) and lower MFI value of PCL ($\text{PCL}_{\text{MFI}} < \text{PLA}_{\text{MFI}}$; $5.57\text{ g/10 min} < 15.84\text{ g/10 min}$) also influence the deformation and droplet size of the dispersed phase during mixing. Consequently, PLA droplets tend to be small, whereas PCL droplets tend to be large.

In addition, Fig. 3(a) shows large standard deviation (error bar) around 50, 60, and 70 wt% PLA content, indicating the irregular droplets sizes and phase inversion around those PLA/PCL compositions. In the case of 50PLA/50PCL, the co-continuous phase morphology behavior is noted for both polymers, with some irregular droplet distributions accompanied by the largest error bars [Fig. 3(a)]. However, it is not possible to detect the phase-separated morphologies by SEM for equal components. Therefore, local TEM analyses were conducted for these morphologies. In Fig. 3(b-d), PLA is shown as light-grey phase, and PCL as the dark phase in the form of strain-like

structures. Two-phase separated morphology is noted for all the blends, 70PLA/30PCL, 60PLA/40PCL, and 50PLA/50PCL. The co-continuous morphology of both PLA and PCL with few irregular strain distributions is clearly detected [Fig. 3(d)], corroborating the SEM images. It is important to note that PCL was partially or occasionally dispersed in PLA; this suggests that the droplets that were observed in the SEM images are related to PCL (50PLA/50PCL composition). This behavior, as well as the large dispersed PCL domain in the PLA-rich samples, reveals that PCL controls the morphology development.

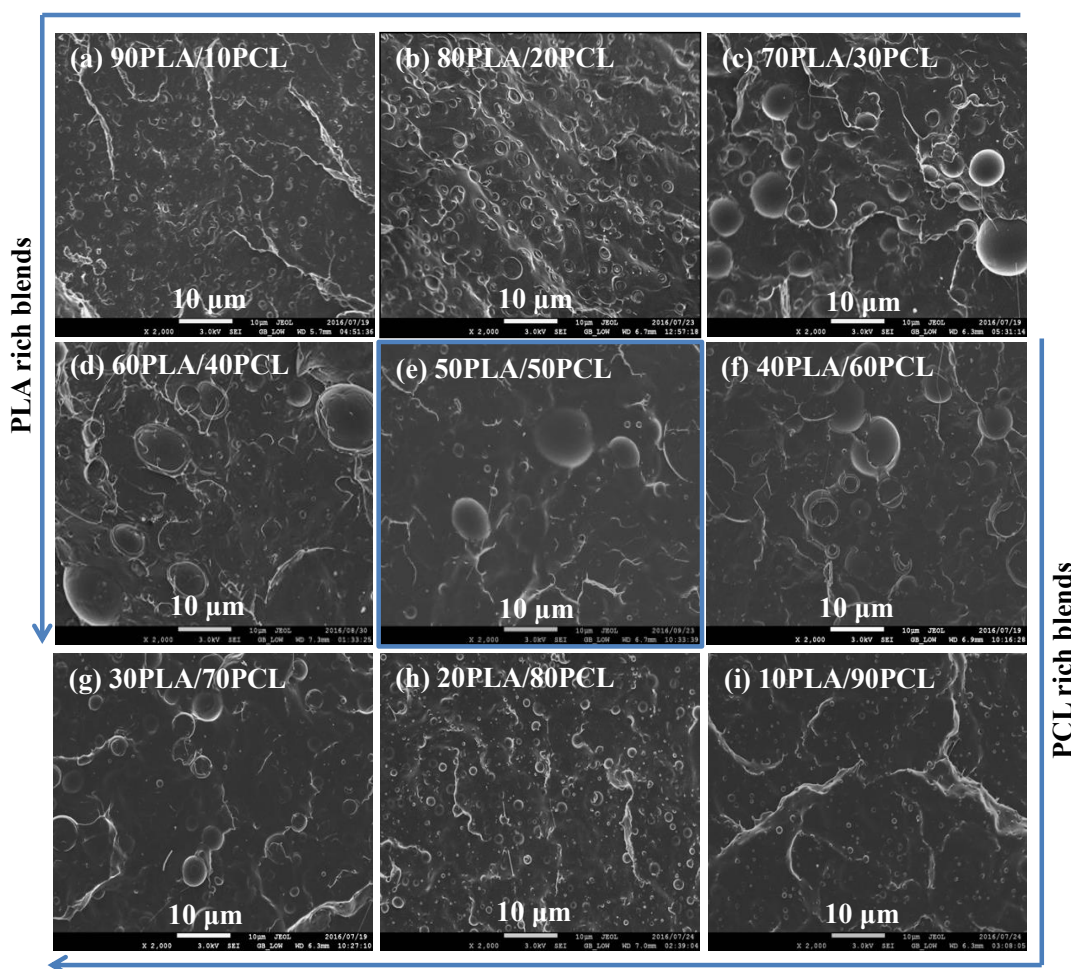


Fig. 2. SEM images of various PLA/PCL blends magnified at 10 μm , x2.000.

The overall morphology of the blends indicates immiscible behavior, which strongly correlates with the XRD patterns and Fourier-transform infrared spectroscopy (FTIR) as well as DMA results, as a result of the governing entropy of mixing between the two polymer matrices [Fig. S1, Supporting Information]. A slight chemical interaction (some sort of chemical interaction)

between the two polymers is presented by FTIR spectra [Fig. S1, Supporting Information], which concur and contributes to the development of immiscible microstructure and material properties increase.

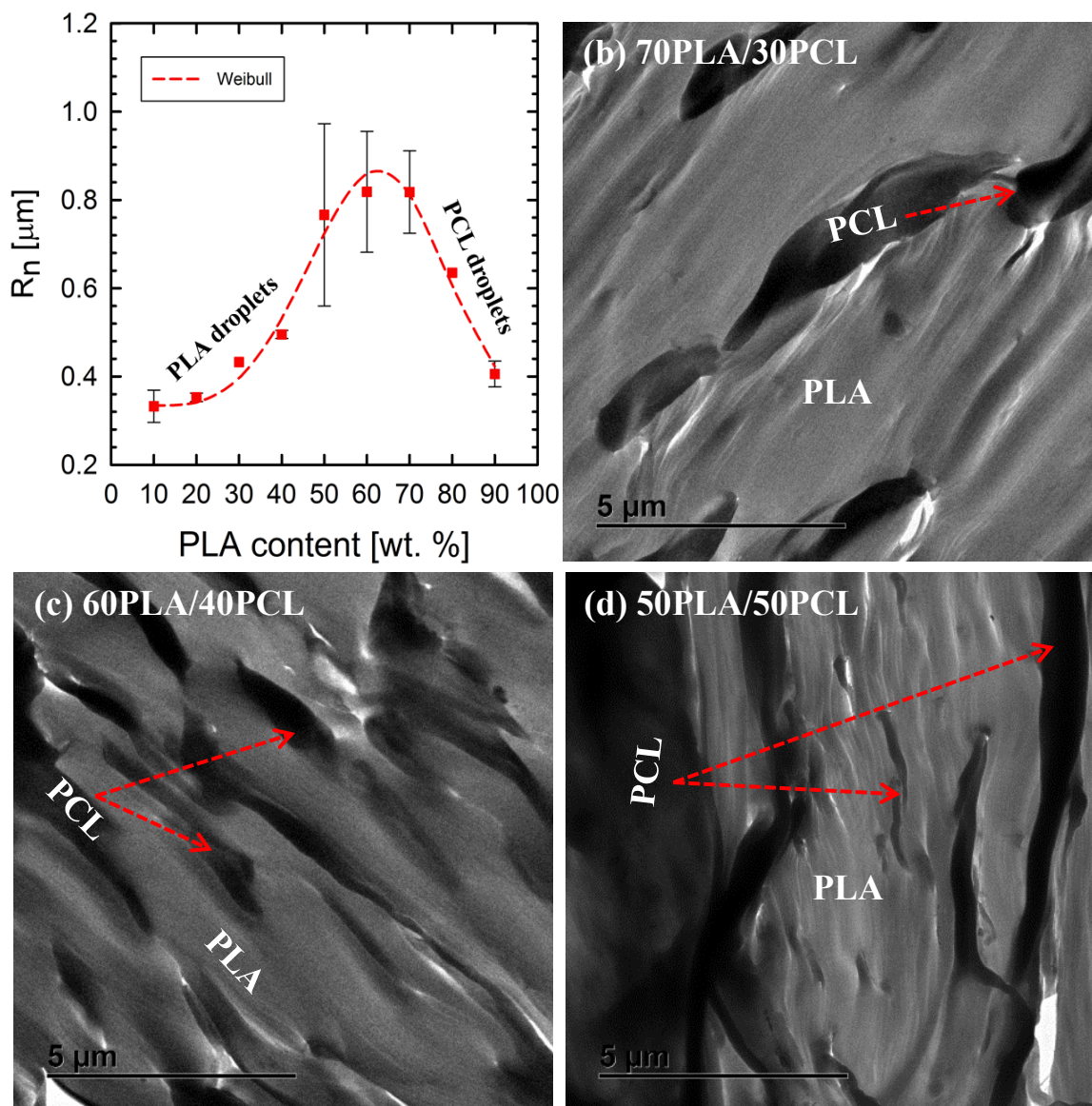


Fig. 3. (a) Number-average radius of PLA and PCL droplets obtained from Fig. 2, and TEM images of (b) 70PLA/30PCL, (c) 60PLA/40PCL, and (d) 50PLA/50PCL blends.

3.2. Thermal stability of PLA/PCL blends by TGA

Fig. 4 shows the thermogravimetric analysis (TGA) (a) and differential thermogravimetric (dTGA) (b) curves of PLA, PCL, and their blends. Table 1 presents the thermal parameters, such as temperature at 10% weight loss ($T_{10\%}$), $T_{50\%}$, and maximum degradation temperature (T_{max}).

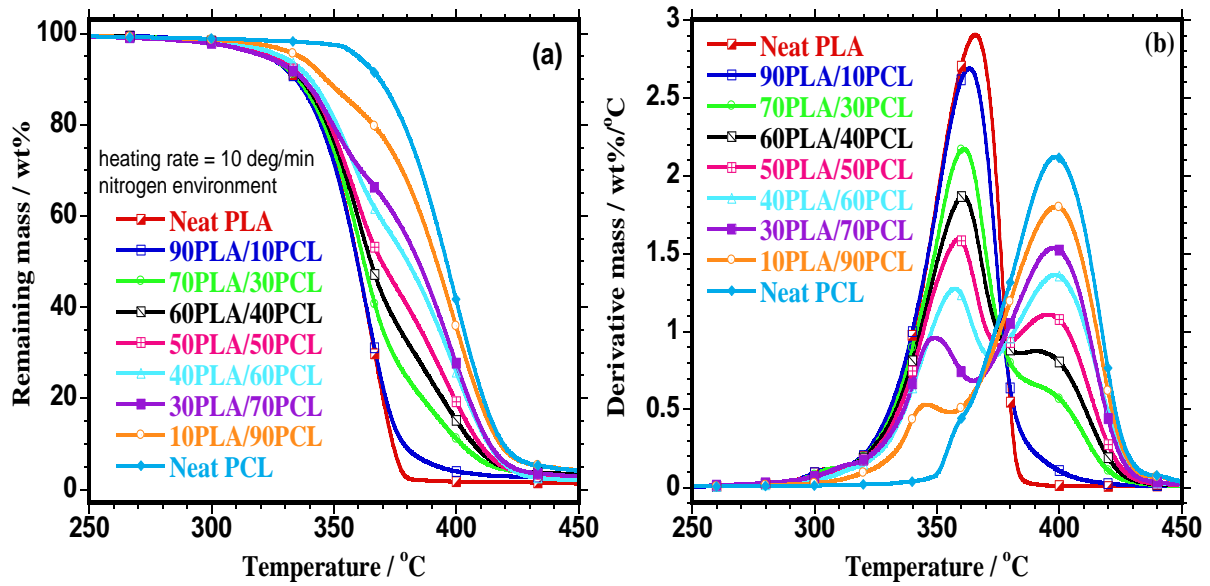


Fig. 4. TGA (a) and dTG (b) curves of neat PLA, PCL, and PLA/PCL blends.

Table 1. Thermal analysis parameters for neat PLA, PCL, and their blends.

| Samples | $T_{10\%}$ (°C) ^a | $T_{50\%}$ (°C) ^a | $T_{max.}$ (°C) ^a :PLA | $T_{max.}$ (°C) ^a :PCL |
|-------------|------------------------------|------------------------------|-----------------------------------|-----------------------------------|
| Neat PLA | 335.22 ±1.51 | 358.09 ±0.12 | 364.15 ±2.06 | - |
| 90PLA/10PCL | 334.14 ±1.63 | 358.18 ±1.26 | 363.19 ±2.46 | - |
| 80PLA/20PCL | 334.14 ±2.59 | 360.00 ±2.74 | 361.93 ±2.65 | - |
| 70PLA/30PCL | 334.15 ±2.26 | 362.13 ±3.68 | 361.06 ±3.36 | 380.50 ±2.12 |
| 60PLA/40PCL | 336.20 ±3.72 | 364.92 ±4.28 | 360.53 ±4.50 | 390.84 ±1.53 |
| 50PLA/50PCL | 336.29 ±2.97 | 369.20 ±1.94 | 358.74 ±2.34 | 395.38 ±3.62 |
| 40PLA/60PCL | 340.04 ±2.39 | 380.26 ±3.62 | 357.26 ±2.51 | 398.31 ±4.17 |
| 30PLA/70PCL | 337.90 ±2.90 | 384.23 ±3.22 | 349.07 ±3.18 | 397.56 ±2.15 |
| 20PLA/80PCL | 342.83 ±1.35 | 390.10 ±2.00 | 348.62 ±1.55 | 398.51 ±2.53 |
| 10PLA/90PCL | 346.51 ±1.76 | 391.91 ±2.98 | 345.76 ±1.87 | 398.81 ±3.85 |
| Neat PCL | 368.20 ±1.26 | 395.92 ±2.00 | - | 398.46 ±1.51 |

^a $T_{10\%}$, ^a $T_{50\%}$, and ^a T_{max} obtained from the TGA curves at a heating rate of 10 °C min⁻¹.

It is noted that neat PLA shows a single degradation step at about 364 °C, whereas neat PCL shows a single degradation step at about 398 °C [20], as clearly visible in Fig 4(b). The PLA/PCL blends show two well-defined degradation steps, and the extent weight loss and degradation steps correspond to the respective content of each polymer within the blends. This confirms the immiscibility of the two polymers that was earlier defined as two-phase separated morphology [Fig. 2 and 3]. It was expected that blending PLA with PCL would increase the thermal stability of their blends throughout the tested temperature range, but this was not the case. Slight thermal stability reduction is noted at $T_{10\%}$ for 90PLA/10PCL, 80PLA/20PCL, and 70PLA/30PCL

compositions contrary to that of neat PLA (Table 1). The reduction is attributed to thermal energy transfer between the PLA matrix and PCL dispersed droplets phase. Interestingly, higher PCL content increases the thermal stability at $T_{10\%}$ for 60PLA/40PCL, 50PLA/50PCL, 40PLA/60PCL, 30PLA/70PCL, 20PLA/80PCL, and 90PLA/10PCL blends. Thermal stability increase is noted for all blends at $T_{50\%}$ (Table 1), relative to neat PLA. This is attributed to the higher thermally stable PCL component. . The optimum thermal stability was shown by 60PLA/40PCL, examining the PLA-rich blends at both $T_{10\%}$ and $T_{50\%}$. As expected, dilution factors led to lower thermal stability of all the blends, compared with that of neat PCL. Briefly, less thermally stable PLA degrades sooner and develops voids; as a result, PCL began to degrade at the edges of those voids. The imaginary holes were observed from SEM images as PLA droplets in PCL-rich blends; however, in TGA analyses they are recognized as degradation gases such as carboxyl groups, the hydroxyl end of polymer chains.

On the other hand, it is notable that the thermal degradation at T_{max} of both polymers in the blends decreases with increasing content of the other polymer. As a result, the degradation temperatures of the blends were not between those of the neat polymers [Fig 4(b) and Table 1]. Mofokeng and Luyt [26] postulated similar degradation behavior based on neat PLA/PCL blends. In addition, the dTGA curves less intensive peaks from neat PLA to 10PLA/90PCL, and from neat PCL to 90PLA/10PCL, indicating the content of each polymer in the blends.

To support the above findings and obtain more insights into the thermal degradation of PLA/PCL counterparts, thermal degradation kinetics studies were carried out. TGA kinetic curves are reported in the supporting information [Fig. S2, Supporting Information]. According to the Kissinger method, the plot of $-\ln(\beta/T_m^2)$ versus $1/T_m \times 10^3$ should be a straight line, therefore the E_a can be evaluated from the slope, which is the minimum energy required to initiate the thermal degradation process [27–29]. Fig. 5 shows the $-\ln(\beta/T_m^2)$ versus $1/T_m \times 10^3$ linear plots of neat PLA, PCL, 60PLA/40PCL, 50PLA/50PCL, and 40PLA/60PCL blends, and the E_a values are summarized in Table 2. As shown in Fig. 5, the Kissinger equation appears feasible for validation,

providing relatively smooth fitting of the points to a straight line with acceptable R^2 values. In addition, it is notable that thermal degradation increases with heating rate in all the samples [Fig. S2(a-e), Supporting Information]. For the E_a profiles, neat PLA exhibits lower E_a value relative to that of neat PCL, at 134.58 and 155.17 KJ mol^{-1} , respectively. This concurs with the high thermal stability of neat PCL resulting from its longer chain length, repeating units attached with well-spaced ‘= O’ functionalities. **The E_a obtained for both PLA and PCL components were as good as to other E_a values reported in the literature for PLA and PCL, which are noted around 26.3 kcal mol^{-1} (110.11 KJ mol^{-1}) and 131 KJ mol^{-1} , respectively [25,26]. The high degree of E_a values suggest that the process was reaction limited rather than being diffusion limited [25].** The PLA/PCL blends are characterized by two E_a profiles, resulting from the immiscibility phenomenon. Briefly, E_{a1} is associated with the first-step degradation of the PLA component (T_{m1}), whereas E_{a2} is associated with the second-step degradation of the PCL component (T_{m2}). It is notable that the introduction of PCL into PLA increased the E_{a1} profiles of 60PLA/40PCL and 40PLA/60PCL blends but not the 50PLA/50PCL composition. This suggests that the governing mechanism changes during the degradation process due to variation of thermally sensitive PLA counterparts within the blends, resulting in low chemical regularity of whole chains and chain interactions [11]. The significant decrement of E_{a1} profiles for the 50PLA/50PCL blend suggests poor morphological factors, such as interfacial interaction of the equivalent thermodynamically immiscible components, as indicated by the error bars for larger droplets [Fig. 3(a)]. Adding PCL to the blend gradually increases the E_{a2} profiles (Table 2). In addition, it is noted that, overall, E_a is mainly controlled by PCL component, resulting from morphological aspects as discussed in section 3.1. The linear increase of E_a characteristics is suppressed by the thermodynamically immiscibility factors resulting from insignificant chemical interaction between the PLA and PCL components [Fig. S1, Supporting Information]. This implies that interaction and morphology play vital roles in the transfer of thermal degradation properties. Moreover, α_{\max} of neat PLA, PCL, and their blends corresponding to T_{m1} and T_{m2} reactions at $15\text{ }^\circ\text{C min}^{-1}$ are summarized in Table 2.

PLA exhibits high α_{\max} relative to neat PCL, indicating that PLA degrades faster than PCL; hence, lower E_a is noted for neat PLA. For the blends, the α_{\max} relating to PLA is higher than that of PCL (e.g., 60PLA/40PCL, $\alpha_{\max1} = 0.60$ and $\alpha_{\max2} = 0.49$). The presence of two different α_{\max} values reveals that PLA/PCL blends degrade in two steps that follow two different mechanisms and order.

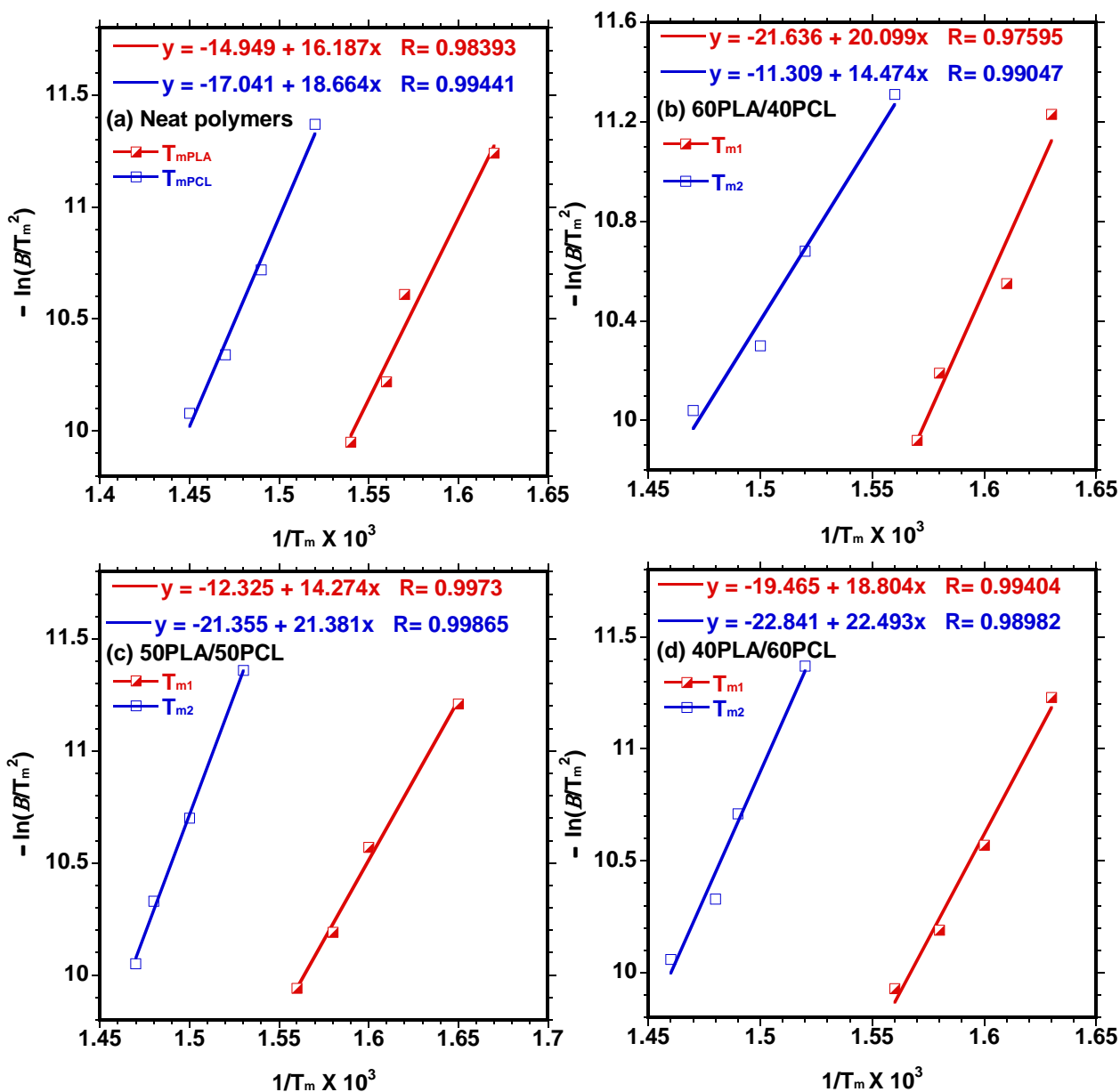


Fig. 5. Kissinger plots of $-\ln(\beta/T_m^2)$ versus $1/T_m \times 10^3$ of neat PLA, PCL, 60PLA/40PCL, 50PLA/50PCL, and 40PLA/60PCL blends.

Table 2. Thermal analysis parameters for neat PLA, PCL, and their blends.

| Samples | E_{a1} (KJ mol ⁻¹) ^a | E_{a2} (KJ mol ⁻¹) ^b | α_{max1} | α_{max2} |
|-------------|---|---|-----------------|-----------------|
| Neat PLA | 134.58 | - | 0.69 | - |
| 60PLA/40PCL | 167.10 | 120.34 | 0.60 | 0.49 |
| 50PLA/50PCL | 118.67 | 177.76 | 0.65 | 0.54 |
| 40PLA/60PCL | 156.34 | 187.01 | 0.65 | 0.54 |
| Neat PCL | - | 155.17 | - | 0.61 |

^a PLA E_{a1} profiles from first step; ^b PCL E_{a2} profiles from second step.

3.3 Melting, crystallization, nonisothermal crystallization kinetics, and spherulitic growth behavior

Fig. 6 shows the cooling (a) and heating (b) curves of neat PLA, PCL, and their various blends obtained from DSC. The T_c , T_m , T_{cc} , and ΔH values obtained from Fig. 6 are summarized in Table 3, while T_g is not discussed here due to insufficient rate (10 °C min⁻¹) and some overlay characteristics. Neat PLA is characterized by a relatively broad T_c peak at high temperature profiles (101.47 °C), while neat PCL is characterized by a sharp crystallization peak at low temperature profiles (27.23 °C). The sharp peak observed in the low-temperature region suggests closely-packed thin-lamellar of PCL, while the broad peak observed in the high-temperature region related to the formation of thick lamellar of PLA. Blending PLA with PCL changed their inherent crystallization behaviors [Fig. 6(a) and Table 3]. The T_c peak of the PCL phase shifted to the lower-temperature profiles, particularly at lower PCL content, whereas the T_c peak of the PLA phase disappeared at lower PLA contents. This implies that the melted PCL particles cover the tiny PLA droplets due to dilution factor. The disappearance of the PLA peak concurs with the XRD diffraction patterns at low PLA content. PLA exhibits less intense T_{cc} peak at about 95 °C. The peak position is slightly affected upon blending with PCL. Furthermore, the intensity varies with PLA-related T_c intensity and PCL content within PLA/PCL blends. Both T_m peaks of PLA and PCL phases are not significantly affected, which is attributed to the degree of immiscibility between PLA and PCL. However, ΔH_m displayed extensively change that was directly proportional to the neat polymer component content. It is notable in Table 3 that the degree of crystallinity of PCL gradually decreases with increasing PLA content, while the crystallinity of

PLA increases slightly with increasing PCL content to some extent. Clearly, high PCL content significantly decreases the crystallinity of PLA, 20PLA/80PCL, and 10PLA/90PLA blends (Table 3). This means that the large nucleus induced by PCL molecules inhibits the mobility of PLA chains. As a result, chain rearrangement is limited, so T_c delay and low X_c are noted. Therefore, it is concluded that the incorporation of low PCL content is sufficient to activate the crystallization of PLA. Todo *et al.* [14] also suggested the possibility of activating PLA crystallization by introducing PCL. Furthermore, similar T_m and X_c behaviors were previously reported by Derakhshandeh *et al.* [35], particularly for PLA/PCL blends.

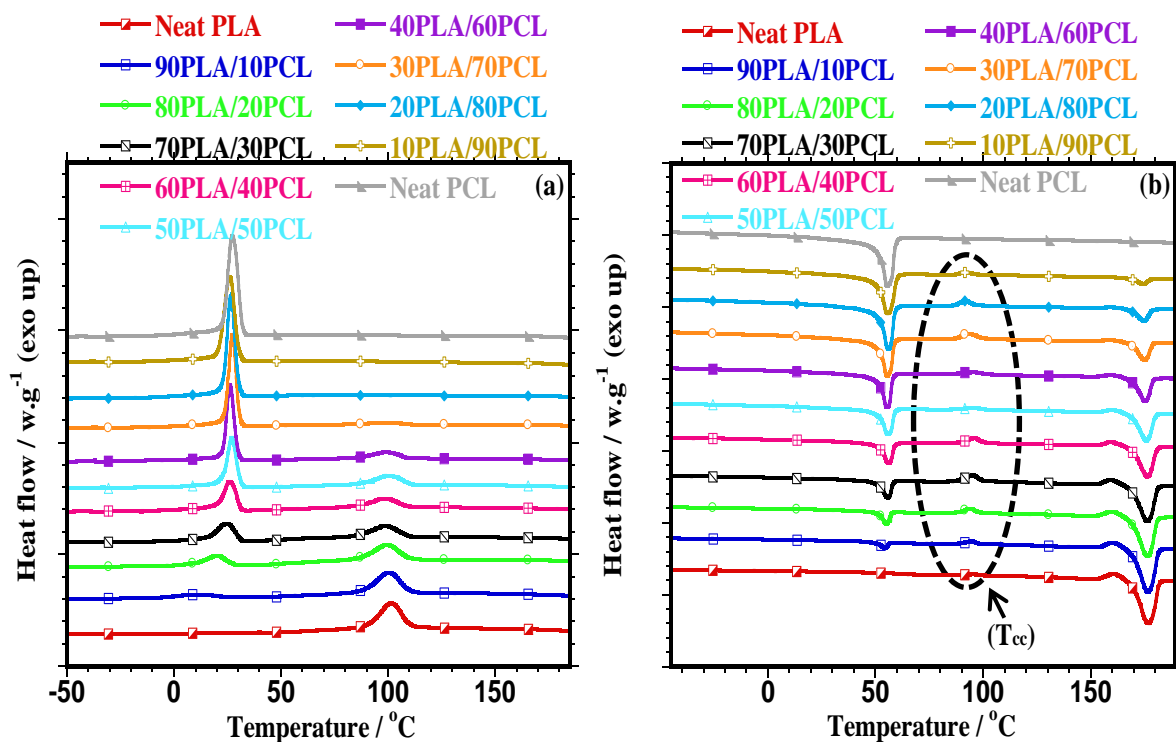


Fig. 6. DSC (a) cooling and (b) second heating curves of neat PLA, PCL, and their blends.

Table 3. DSC data obtained from cooling and second heating curves.

| Samples | T_{cc} ($^{\circ}\text{C}$) | ΔH_{cc} ($\text{J}\cdot\text{g}^{-1}$) | T_c ($^{\circ}\text{C}$) ^a | ΔH_c ($\text{J}\cdot\text{g}^{-1}$) ^a | T_m ($^{\circ}\text{C}$) ^a | ΔH_m ($\text{J}\cdot\text{g}^{-1}$) ^a | X_c (%) ^a |
|-------------|---------------------------------|--|---|--|---|--|------------------------|
| Neat PLA | 95.87 \pm 0.12 | 1.49 \pm 0.15 | 101.47 \pm 0.16 | 31.40 \pm 1.36 | 176.91 \pm 0.01 | 55.26 \pm 0.32 | 59.42 |
| 90PLA/10PCL | 94.85 \pm 0.06 | 2.35 \pm 0.25 | 100.18 \pm 0.40 | 27.26 \pm 0.24 | 176.63 \pm 0.13 | 51.44 \pm 0.72 | 61.46 |
| | | | 10.82 \pm 0.71 | 4.983 \pm 0.06 | 54.62 \pm 0.16 | 3.37 \pm 0.29 | 24.96 |
| 80PLA/20PCL | 94.61 \pm 0.29 | 4.70 \pm 0.22 | 99.50 \pm 0.83 | 22.75 \pm 1.48 | 176.59 \pm 0.25 | 46.42 \pm 0.53 | 62.39 |
| | | | 19.09 \pm 0.29 | 11.80 \pm 0.10 | 55.29 \pm 0.16 | 7.73 \pm 0.52 | 28.63 |
| 70PLA/30PCL | 95.30 \pm 0.14 | 7.71 \pm 0.04 | 98.09 \pm 0.21 | 16.42 \pm 0.21 | 176.52 \pm 0.16 | 40.07 \pm 0.81 | 61.55 |
| | | | 22.90 \pm 3.13 | 18.20 \pm 0.38 | 55.68 \pm 0.21 | 12.16 \pm 0.13 | 30.02 |
| 60PLA/40PCL | 96.07 \pm 0.15 | 6.11 \pm 0.27 | 97.80 \pm 0.16 | 13.46 \pm 0.56 | 176.42 \pm 0.10 | 32.53 \pm 0.47 | 58.30 |
| | | | 26.38 \pm 0.54 | 22.90 \pm 0.33 | 56.13 \pm 0.07 | 17.23 \pm 0.17 | 31.91 |
| 50PLA/50PCL | 96.53 \pm 0.128 | 4.18 \pm 1.05 | 99.48 \pm 0.04 | 13.24 \pm 0.99 | 175.78 \pm 0.06 | 30.01 \pm 0.10 | 64.54 |
| | | | 27.02 \pm 0.01 | 32.01 \pm 1.40 | 55.83 \pm 0.11 | 25.03 \pm 0.82 | 37.08 |
| 40PLA/60PCL | 95.87 \pm 0.20 | 4.09 \pm 0.43 | 98.57 \pm 0.11 | 9.45 \pm 0.30 | 175.49 \pm 0.10 | 23.69 \pm 0.12 | 63.68 |
| | | | 26.50 \pm 0.30 | 37.58 \pm 0.71 | 55.34 \pm 0.07 | 32.08 \pm 0.23 | 39.60 |
| 30PLA/70PCL | 93.50 \pm 0.01 | 7.00 \pm 0.33 | - | - | 175.21 \pm 0.15 | 17.10 \pm 0.08 | 63.41 |
| | | | 27.47 \pm 0.16 | 44.59 \pm 2.99 | 55.42 \pm 0.12 | 38.67 \pm 1.06 | 40.92 |
| 20PLA/80PCL | 91.89 \pm 0.10 | 5.21 \pm 0.20 | - | - | 174.71 \pm 0.15 | 10.42 \pm 0.13 | 56.02 |
| | | | 26.85 \pm 0.20 | 50.12 \pm 1.61 | 55.66 \pm 0.23 | 46.59 \pm 1.97 | 43.14 |
| 10PLA/90PCL | 92.63 \pm 0.63 | 2.18 \pm 0.11 | - | - | 174.60 \pm 0.09 | 4.61 \pm 0.27 | 49.57 |
| | | | 25.43 \pm 0.59 | 56.97 \pm 0.30 | 55.44 \pm 0.23 | 54.93 \pm 0.53 | 45.21 |
| Neat PCL | - | - | 27.23 \pm 0.06 | 64.03 \pm 2.43 | 55.48 \pm 0.02 | 62.63 \pm 1.64 | 46.39 |

^aTop values within the blocks represent PLA temperature profiles; whereas bottom values represent PCL temperature profiles.

The effect of cooling rate on the crystallization rates of PLA-based blends was studied at 5, 10, 15, and 20 °C min⁻¹ and the curves are presented in Fig. S3 (Supporting Information). It is noted that the T_c peak related to neat PLA and PCL decreases with faster cooling rates. The same behavior is noted in the blends. This suggests that at lower cooling rates there is sufficient time to overcome the nucleation barrier, so high T_c is observed [36]. Slowing the cooling rate increases the nuclei density of the blends. This concurs with the absence of T_{cc} peak at slower cooling rates [Fig. S4, Supporting Information]. In addition, the activation of PLA crystallization was explored through crystallization rate coefficient (CRC) adapted from Liu *et al.* [36]. The CRCs were measured from the slope of the nonisothermal crystallization plots of various cooling rates versus T_c [Fig. S3, Supporting Information]. The linear plots of nonisothermal crystallization kinetics are shown in Fig. 7, and the CRCs are summarized in Table 4. Neat PLA has lower CRC than neat PCL. Interestingly, the CRCs of the blends are higher than that of the neat PLA, due to the introduction of neat PCL with high CRC. Fundamentally, higher CRC indicates faster crystallization [36]. Therefore, the enhanced CRCs of the blends confirm the activation of PLA crystallization by introduction of PCL. Importantly, the optimum CRC is archived at 60PLA/40PCL.

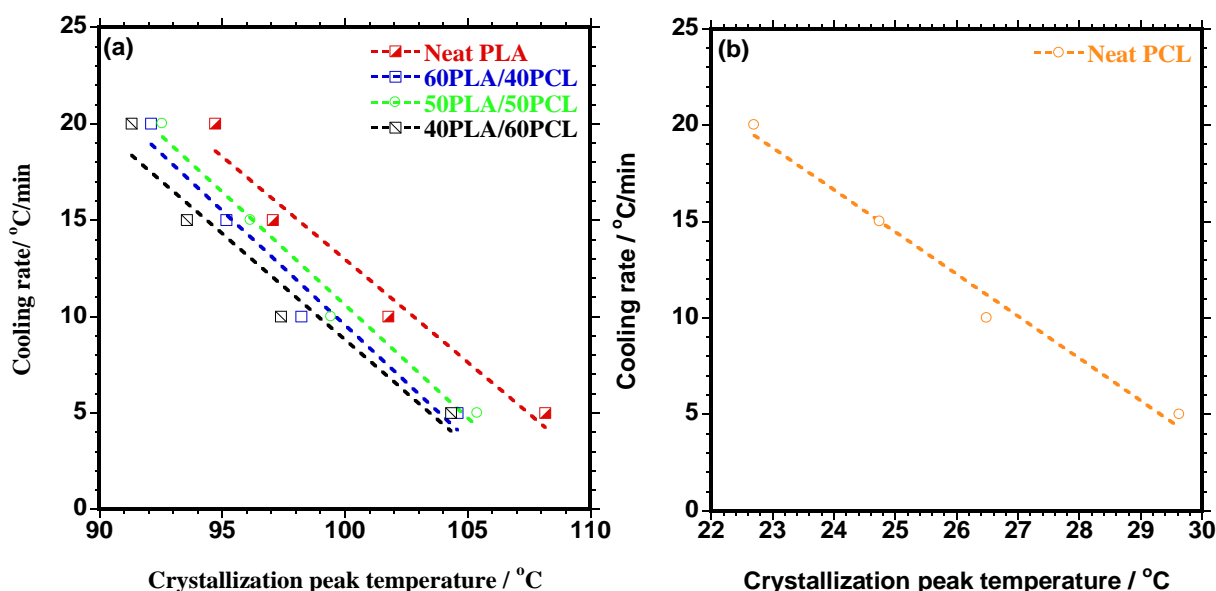


Fig. 7. Linear plots of nonisothermal crystallization kinetics of PLA-based blends.

Table 4. CRC data obtained from nonisothermal cooling process [Fig. S3, Supporting Information].

| Samples | R ² value | Slope | CRC (h ⁻¹) |
|-------------|----------------------|-------|------------------------|
| Neat PLA | 0.98 | -1.07 | 64.00 |
| 60PLA/40PCL | 0.98 | -1.19 | 71.17 |
| 50PLA/50PCL | 0.99 | -1.17 | 70.32 |
| 40PLA/60PCL | 0.97 | -1.10 | 66.01 |
| Neat PCL | 0.99 | -2.18 | 130.84 |

Fig. 8 shows the nucleation effect of the PCL particles, and spherulite evolution during the melt crystallization of PLA in the blends as examined by local POM, first isothermally crystallized at 120 °C for PLA (for all selected samples) and further isothermally crystallized at 30 °C for neat PCL. In Fig. 8(a), neat PLA lacks nucleation sites relative to the blends, which is attributed to its inherent slow crystallization rate indicated by lower CRC relative to that of the neat PCL and the blends (Table 4). No spherulites are observed for neat PCL, due to its lower T_m profiles (at 5 min, isothermally crystallized 120 °C). In the blends [Fig. 8(c – e)], PLA spherulites start to grow along the edges of molten PCL, which acts as a nucleation site for PLA crystals. In addition, the PLA/PCL blends have a higher number of nucleation sites compared to neat PLA and hence a faster crystallization rate. After 20 min isothermal crystallization at 120 °C, neat PLA exhibits significantly large spherulites, whereas no spherulites were observed for neat PCL at 120 °C, since it was still in its melt state. However, very small and more densely packed crystallites were observed at 30 °C [Fig. 8(b’)]. This corroborates the lower T_c and T_m profiles shown in the DSC section [Fig. 6, Table 3]. The PLA/PCL blends exhibit significantly smaller spherulites relative to neat PLA. This indicates that the PCL particles dispersed into the PLA matrix act as a nucleating agent for PLA crystallization. This is evident by the increase in the number of nuclei, thus the formation of small spherulites, which corroborates the CRC (Table 4) [37]. Furthermore, the addition of more PCL particles enhanced spherulites border line, indicating that the characteristic was content-dependent.

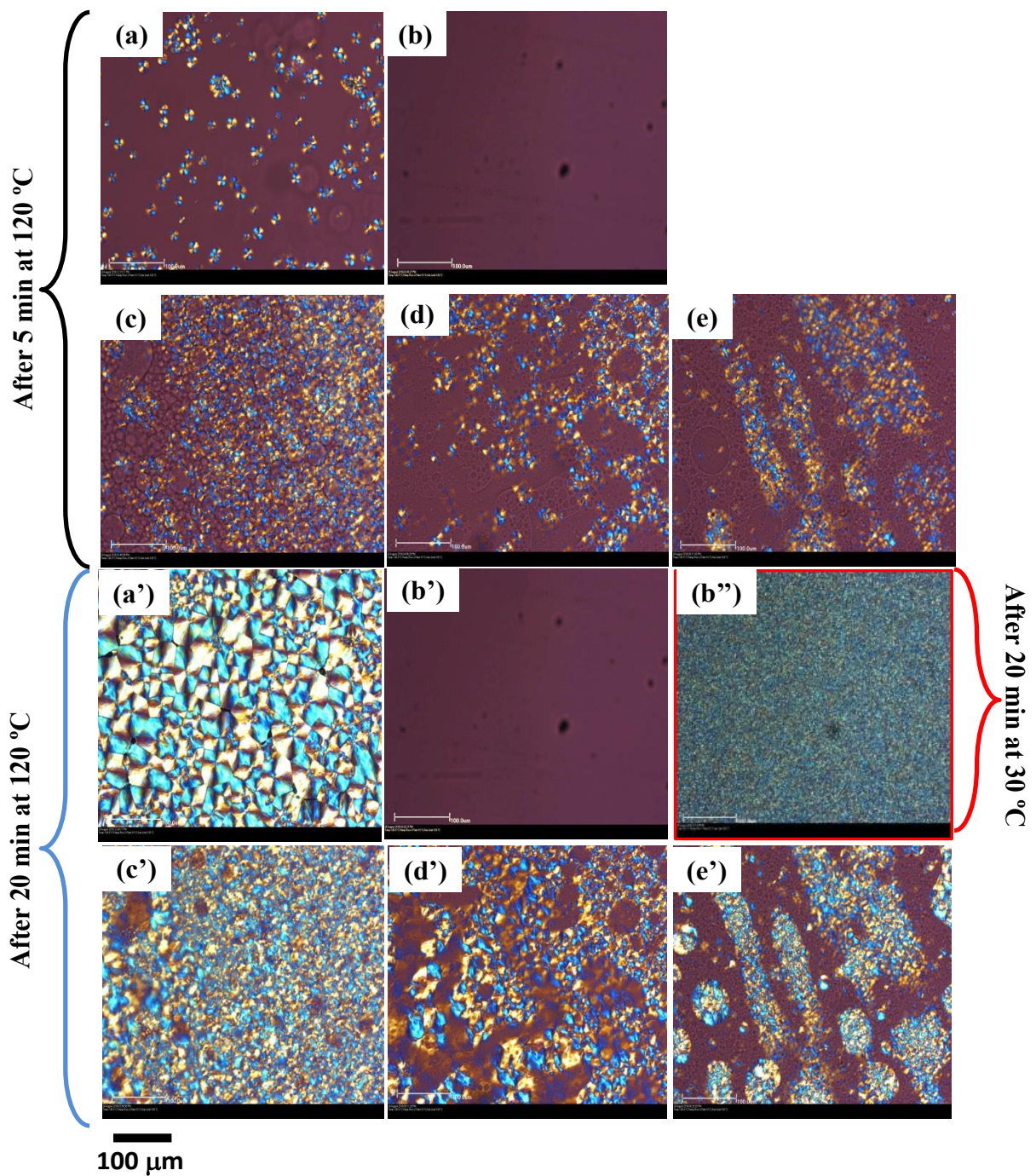


Fig. 8. POM images taken during isothermal melt-crystallization at 120 °C after 5 min: (a) neat PLA, (b) neat PCL, (c) 60PLA/40PCL, (d) 50PLA/50PCL, (e) 40PLA/60PCL; and further at 120 °C after 20 min: (a') neat PLA, (b') neat PCL, (c') 60PLA/40PCL, (d') 50PLA/50PCL, (e') 40PLA/60PCL; and at 30 °C after 20 min: (b'') neat PCL only.

3.4. Dynamic mechanical properties

Fig. 9(a) presents the storage modulus (E') curves of neat PLA, PCL, and their blends, while the tan delta curves are presented in Fig. 9(b) and (b'). The T_g profiles for neat PLA and PCL are observable at about 67 °C and -42 °C. Similar T_g profiles were previously observed by Lopez-Rodriguez *et al.* [38]. In the blends, two distinguishable T_g peaks are observable within the same region as that of their respective neat polymers, clearly indicating immiscibility between the two polymers. The increasing and decreasing of the tan delta peak intensity reflect the blend compositions. E' curves are divided into four regions (I–IV). Region (I) is below the T_g of both polymers, and is therefore denoted as a glassy region. Along region (I), the molecules of both polymers are frozen and chain mobility is limited due to low internal energy. Therefore, both polymers show relatively high E' at region (I) compared that at high temperatures or other regions along the test. Furthermore, neat PCL exhibits high E' ($E'_{PCL} > E'_{PLA}$) relative to neat PLA in region (I) due to its high packing density and semi-crystalline nature. Region (II) is a cross-over region in which both PCL and PLA are still below their T_g . E' of PCL significantly decreases with increasing temperature, since it is very close to its T_g . Therefore, chain relaxation is improved as a result of the orientation of lamellar structures due to temperature sensitivity. A slight decrease in E' is seen for neat PLA, since its chain mobility is still limited due to its high T_g . Region (III) is denoted as PCL T_g , while region (IV) is denoted as PLA T_g , clearly shown in Fig. 9(b), in which PCL is in a rubbery state. Along these regions (III and IV), neat PCL exhibits lower E' relative to neat PLA due to the chain relaxation phenomena and unfrozen molecules. In comparison, molecules are still frozen, thus having low internal energy which limits the movement of PLA chains below its T_g ; hence, PLA is brittle at room temperatures. In the PLA/PCL blends, stiffness, toughness, and flexibility are dependent on the contents of the constituent polymers, since the blends are an immiscible system of more ductile and brittle polymer.

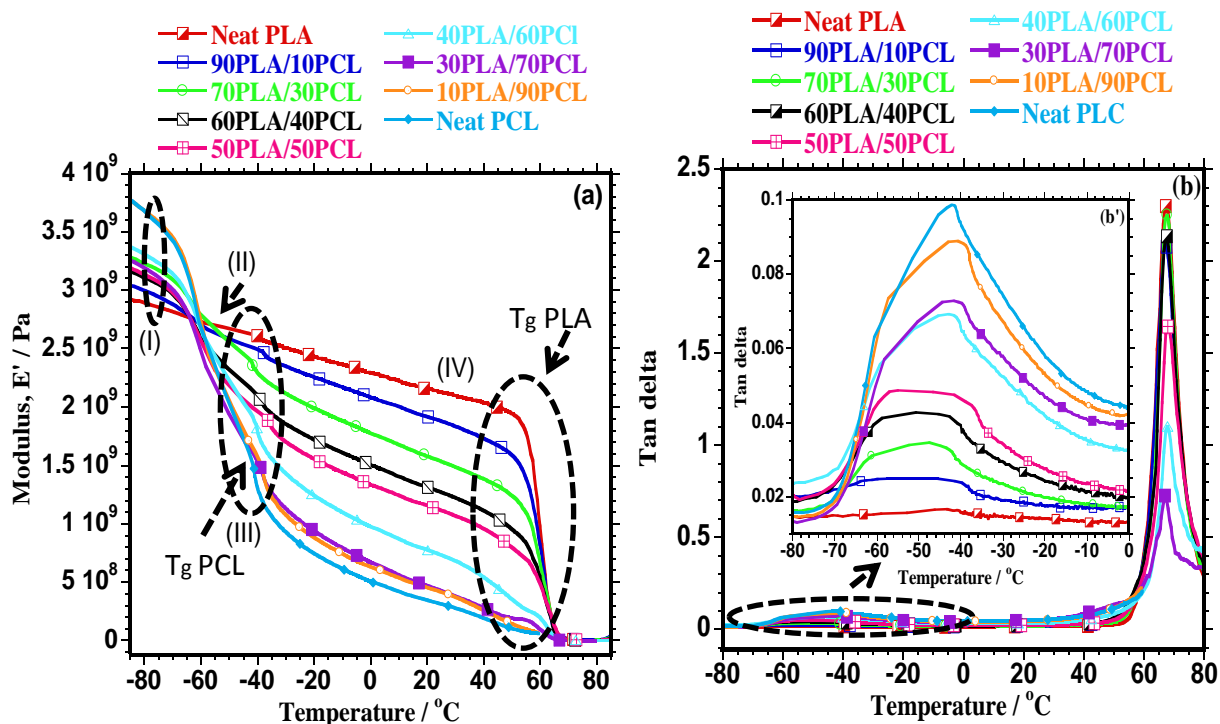


Fig. 9. DMA storage modulus (a) and tan delta (b) curves of neat PLA, neat PCL, and their blends.

3.5. Tensile properties

From Fig. 10, high tensile modulus, high tensile strength, and low elongation at break are observed for neat PLA, which is attributed to its glassy state around room temperature related to its high T_g of 67 °C [Fig. 9] as well as its large spherulites and short repeating units. A low tensile modulus is observed for neat PCL, because of its low T_g of -42 °C the internal energy is sufficient to allow chain mobility [Fig. 9], so high level of deformation around room temperatures is possible. In the blends, tensile modulus and tensile strength reduction is noted with higher PCL content. However, the inherent PCL ductility benefits the blends by systematically increasing the system's elongation at break. In addition, the system indicates two-phase separated morphology throughout; the strong phase separation is observable in rich PCL blends by not following the mixing line rule. Briefly, all of the blends exhibited immiscibility and none followed the mixing rule [Fig. 10(b)]. Importantly, the composition of the 60PLA/40PCL blend is relatively similar to the mixing line with inherent properties of both polymers, thus balancing the properties, being concurrently tough

and fairly flexible. This is attributed to significantly small spherulites relative to neat PLA, and fairly dispersed spherulites morphology as well as undefined borderline [39]. The perfect borderline significantly influences the elongation at break; however, it negatively affects the tensile modulus and strength characteristics as a result of immiscible behavior. In addition, significantly large spherulites led to brittle behavior of the polymeric materials (neat PLA) [39], while tiny spherulites led to ductile behavior. These findings on tensile properties concur with the DMA results.

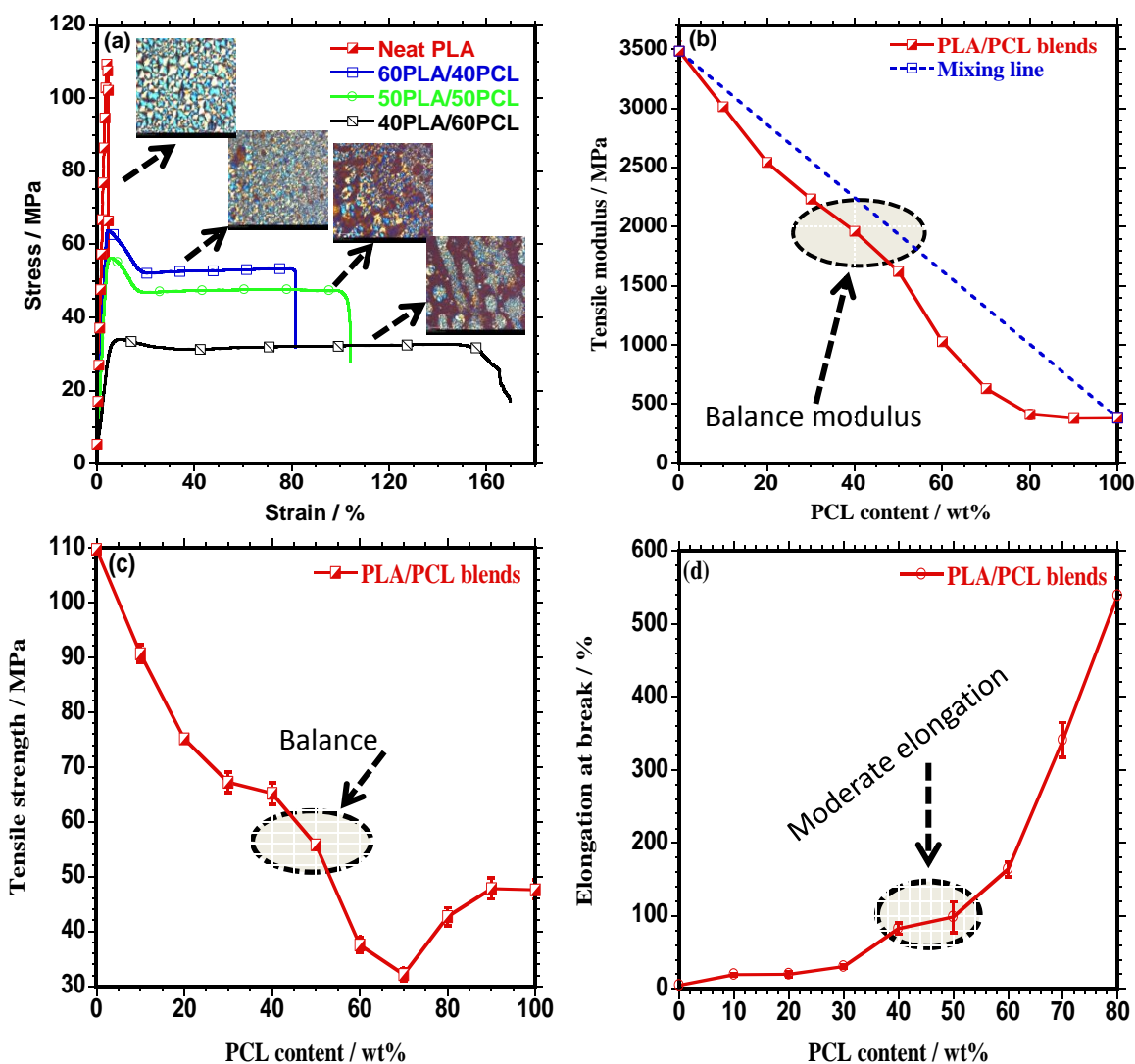


Fig. 10. Stress-strain curves and inset POM images (a), tensile modulus (b), tensile strength (c), and elongation at break (d) of the PLA/PCL blends as a function of PCL content.

4. Conclusions

Blending thermodynamically immiscible PLA and PCL reduced the onset temperature of both polymers, but increased the complete thermal degradation of PLA, indicating the role of highly thermally stable polymer component and activation energies driven by the morphology factors. Neat PLA exhibited lower activation energy than PCL; however, the addition of PCL fine-tuned the activation energy of the blends. CRCs indicated that the addition of PCL particles activated the poor crystallization of PLA resulting from low mobility of PLA chains due to brittle, short repeating units and lack sufficient nucleators. Rheological data revealed that PLA/PCL blends exhibited higher melt elasticity and viscosity relative to that of neat PLA. Interestingly, the 60PLA/40PCL blend showed ideal composition, with intermediate stiffness, strength, remarkably increased elongation at break for PLA-rich blends, thermal stability, and activation energy balance, significant nucleation sites for effective PLA spherulites growth rate, and unique CRC profile. These findings may not only contribute to the development of environmentally friendly, high-performance PLA/PCL blends, but also to the fundamentals of polymer science for the future design of cold and hot polymeric packaging materials, refrigerators, and water drinking flasks.

Supporting Information

Supporting information is available from the authors.

Acknowledgements

The authors appreciate the financial support of the National Research Foundation, South Africa, together with the University of Johannesburg and the Council for Scientific and Industrial Research; and further thank the staff of the DST-CSIR NCNSM characterization facility for their work on characterization.

References

- [1] Y. Tokiwa, B. P. Calabia, C. U. Ugwu, S. Aiba, Biodegradability of plastics, *Int. J. Mol. Sci.* 10 (2009) 3722–3742.
- [2] A. K. Matta, R. U. Rao, K. N. S. Suman, V. Rambabu, Preparation and characterization

- of biodegradable PLA / PCL polymeric blends, *Procedia Mater. Sci.* 6 (2014) 1266–1270.
- [3] F. Signori, M. Coltelli, S. Bronco, Thermal degradation of poly (lactic acid) (PLA) and poly (butylene adipate- co -terephthalate) (PBAT) and their blends upon melt processing, *Polym. Degrad. Stab.* 94 (2009) 74–82.
- [4] M. Nofar, A. Maani, H. Sojoudi, M. C. Heuzey, P. J. Carreau, Interfacial and rheological properties of PLA / PBAT and PLA / PBSA blends and their morphological stability under shear flow, *J. Rheol.* 59 (2015) 317–333.
- [5] M. Deroiné, A. Le Duigou, Y. Corre, P. Le Gac, P. Davies, G. César, S. Bruzaud, Accelerated ageing of polylactide in aqueous environments: Comparative study between distilled water and seawater, *Polym. Degrad. Stab.* 108 (2014) 319–329.
- [6] Y. Xu, Y. Wang, T. Xu, J. Zhang, C. Liu, Crystallization kinetics and morphology of partially melted poly (lactic acid), *Polym. Test.* 37 (2014) 179–185.
- [7] T. Patrício, P. Bártolo, Thermal stability of PCL/PLA blends produced by physical blending process, *Procedia Eng.* 59 (2013) 292–297.
- [8] P. F. M. Finotti, L. C. Costa, T. S. O. Capote, R. M. Scarel-caminaga, M. A. Chinelatto, Immiscible poly (lactic acid)/poly (ϵ -caprolactone) for temporary implants: Compatibility and cytotoxicity, *J. Mech. Behav. Biomed. Mater.* 68 (2017) 155–162.
- [9] V. Ojijo, S. S. Ray, R. Sadiku, “Role of specific interfacial area in controlling properties of immiscible blends of biodegradable polylactide and poly[(butylene succinate)-co-adipate], *ACS Appl. Mater. Interfaces* 4 (2012) 6690–6701.
- [10] R. Homklin, N. Hongsriphan, Mechanical and thermal properties of PLA/PBS co-continuous blends adding nucleating agent, *10th Eco-Energy Mater. Sci. Eng.* 34 (2013) 871–879.
- [11] G. Sivalingam, G. Madras, Thermal degradation of binary physical mixtures and copolymers of poly (3-caprolactone), poly (D, L-lactide), poly (glycolide), *Polym. Degrad. Stab.* 84 (2004) 393–398.
- [12] R. Dell, G. Groeninckx, G. Maglio, M. Malinconico, A. Migliozzi, Immiscible polymer

blends of semicrystalline biocompatible components: thermal properties and phase morphology analysis of PLLA/PCL blends, *Polymer* 42 (2001) 7831–7840.

[13] C.-C. Chen, J.-Y. Chueh, H. Tseng, H.-M. Huang, S.-Y. Lee, Preparation and characterization of biodegradable PLA polymeric blends, *Biomaterials* 24 (2003) 1167–1173.

[14] M. Todo, S.-D. Park, T. Takayama, K. Arakawa, Fracture micromechanisms of bioabsorbable PLLA/PCL polymer blends, *Eng. Fract. Mech.* 74 (2007) 1872–1883.

[15] S. S. Ray, Polylactide-based bionanocomposites: A new class of hybrid materials, *Acc. Chem. Res.* 45 (2012) 1710–1720.

[16] D. Wu, Y. Zhang, M. Zhang, W. Zhou, “Phase behavior and its viscoelastic response of polylactide/poly(ϵ -caprolactone) blend, *Eur. Polym. J.* 44 (2008) 2171–2183.

[17] L. L. Cabelo, J. L. Feijoo, M. P. Villanueva, E. Giménez, Optimization of biodegradable nanocomposites based on aPLA/PCL blends for food packaging applications, *Macromol. Symp.* 233 (2006) 191–197.

[18] G. Sivalingam, G. Madras, Thermal degradation of ternary blends of poly (ϵ -caprolactone) / poly (vinyl acetate)/ poly (vinyl chloride), *J. Appl. Polym. Sci.* 93 (2004) 1378–1383.

[19] K. N. Y. Kodama, L.D.B. Machado, C. Giovedi, Gamma radiation effect on structural properties of PLLA / PCL blends, *Nucl. Instr. Meth. Phys. Res. B* 265 (2007) 294–299.

[20] I. Navarro-Baena, V. Sessini, F. Dominici, L. Torre, J. M. Kenny, L. Peponi, “Design of biodegradable blends based on PLA and PCL: From morphological , thermal and mechanical studies to shape memory behavior, *Polym. Degrad. Stab.* 132 ((2016) 97–108.

[21] A. Ostafinska, I. Fortelny, J. Hodan, S. Krejcikova, M. Nevoralova, J. Kredatusova, Z. Krulis, J. Kotek, M. Slouf, Strong synergistic effects in PLA/PCL blends: Impact of PLA matrix viscosity, *J. Mech. Behav. Biomed. Mater.* 69 (2017) 229–241.

[22] L. Gardella, M. Calabrese, O. Monticelli, PLA maleation: an easy and effective method to modify the properties of PLA/PCL immiscible blends, *Colloid Polym. Sci.* 292 (2014) 2391–2398.

- [23] O. J. Botlhoko, S. S. Ray, J. Ramontja, Influence of functionalized exfoliated reduced graphene oxide nanoparticle localization on mechanical, thermal and electronic properties of nanobiocomposites, *Eur. Polym. J.* 102 (2018) 130–140.
- [24] A. Ostafinska, I. Fortelny, M. Nevoralova, J. Hodan, J. Kredatusova, M. Slouf, Synergistic effects in mechanical properties of PLA/ PCL blends with optimized composition, processing, and morphology, *RSC Adv.* 5 (2015) 98971–98982.
- [25] M.K. Mitchell, D.E. Hirt, Degradation of PLA fibers at elevated temperature and humidity, *Polym. Eng. Sci.* 55 (2015) 1652-1660.
- [26] J. P. Mofokeng, A. S. Luyt, Morphology and thermal degradation studies of melt-mixed poly(lactic acid) (PLA)/poly(ϵ -caprolactone) (PCL) biodegradable polymer blend nanocomposites with TiO₂ as filler, *Polym. Test.* 45 (2015) 93–100.
- [27] Y. Cho, M. Shim, S. Kim, Thermal degradation kinetics of PE by the Kissinger equation, *Mater. Sci. Commun.* 52 (1998) 94–97.
- [28] A. Benarbia, A. Elidrissi, I. Ganetri, R. Touzani, Synthesis, characterization and thermal degradation kinetics of copolyesters, *J. Mater. Environ. Sci.* 5 (2014) 1262–1279.
- [29] F. Huang, Thermal properties and thermal degradation of cellulose tri-stearate (CTs), *Polymer (Guildf)* 4 (92012) 1012–1024.
- [30] J. Ramontja, S. S. Ray, S. K. Pillai, A. S. Luyt, “High-performance carbon nanotube-reinforced bioplastic, *Macromol. Mater. Eng.* 249 (2009) 839–846.
- [31] K. K. Gupta, N. Pal, P. K. Mishra, P. Srivastava, 5-Fluorouracil-loaded poly(lactic acid)-poly(ϵ -caprolactone) hybrid scaffold: Potential chemotherapeutic implant, *J. Biomed. Mater. Res. Part A* 102A (2014) 2600–2612.
- [32] K. Sownthari, S. A. Suthanthiraraj, Synthesis and characterization of an electrolyte system based on a biodegradable polymer, *Xpress Polym. Lett.* 7 (2013) 495–504.
- [33] H. Peng, Y. Han, T. Liu, C. W. Tjiu, C. He, Morphology and thermal degradation behavior of highly exfoliated CoAl-layered double hydroxide/polycaprolactone nanocomposites

prepared by simple solution intercalation, *Thermochim. Acta* 502 (2010) 1–7.

[34] T. G. Mofokeng, V. Ojijo, S. S. Ray, The Influence of Blend Ratio on the Morphology, Mechanical, Thermal, and Rheological Properties of PP/LDPE Blends, *Macromol. Mater. Eng.* 301 (2016) 1191–1201.

[35] M. Derakhshandeh, N. Noroozi, L. L. Schafer, D. Vlassopoulos, S. G. Hatzikiriakos, Dynamics of partially miscible polylactide-poly(ϵ -caprolactone) blends in the presence of cold crystallization, *Rheol. Acta* 55 (2016) 657–671.

[36] T. Liu, W. Lin, M. Yang, S. Chen, Miscibility, thermal characterization and crystallization of poly (L-lactide) and poly (tetramethylene adipate-co-terephthalate) blend membranes, *Polymer* 46 (2005) 12586–12594.

[37] S. S. Ray, K. Yamada, A. Ogami, M. Okamoto, K. Ueda, New polylactide/layered silicate nanocomposite: nanoscale control over multiple properties, *Macromol. Rapid Commun.*, 23 (2002) 943–947.

[38] N. López-Rodríguez, A. López-Arraiza, E. Meaurio, J.R. Sarasua, Crystallization, morphology, and mechanical behavior of polylactide/poly (ϵ -caprolactone) blends, *Polym. Eng. Sci.* 46 (2006) 1299–1308.

[39] H. Li, X. Lu, H. Yang, J. Hu, Non-isothermal crystallization of P (3HB-co-4HB)/PLA blends, *J. Therm. Anal. Calorim.* 122 (2015) 817–829.